REVIEW ARTICLE

Approaches for the optimization of MR protocols in clinical hybrid PET/MRI studies

**Maria-Isabel Vargas · Minerva Becker · Valentina Gariboto ·
Susanne Heinzer · Pierre Loubeyre · Joanna Gariani ·
Karl Lovblad · Jean-Paul Vallée · Osman Ratib**

Abstract Magnetic resonance imaging (MRI) is the examination method of choice for the diagnosis of a variety of diseases. MRI allows us to obtain not only anatomical information but also identification of physiological and functional parameters such as networks in the brain and tumor cellularity, which plays an increasing role in oncologic imaging, as well as blood flow and tissue perfusion. However, in many cases such as in epilepsy, degenerative neurological diseases and oncological processes, additional metabolic and molecular information obtained by PET can provide essential complementary information for better diagnosis. The combined information obtained from MRI and PET acquired in a single imaging session allows a more accurate localization of pathological findings and better assessment of the underlying physiopathology, thus providing a more powerful diagnostic tool. Two hundred and twenty-one patients were scanned from April 2011 to January 2012 on a Philips Ingenuity TF PET/MRI system. The purpose of this review article is to provide an overview of the techniques used for the optimization of different protocols performed in our hospital by specialists in the following fields: neuroradiology, head and neck, breast, and prostate imaging. This paper also discusses the different problems encountered, such as the length of studies, motion artifacts, and accuracy of image fusion including physical and technical aspects, and the proposed solutions.

Keywords MRI · PET · Breast · Head and neck · Prostate · Sequences · Protocols · Tumors · Epilepsy · Dementia

Introduction

It was during the 1990s that Woods and Shao used PET/MRI in small animals for the first time [1, 2], but it was not before 2006 that the first simultaneous MRI and PET images of the human brain were acquired [3, 4]. The main difficulty when using these two techniques together is the interference between the two scanners, resulting in electromagnetic interference of the PET readout electronics with the MRI system and failure of the PET photomultiplier tubes in the magnetic field of the MRI machine [5].

Two different kinds of hybrid PET/MRI systems are currently on the market: one with a sequential acquisition mode (Philips Ingenuity TF PET/MRI) and another with a simultaneous MRI and PET acquisition technique (Siemens Biograph mMR, Erlangen, Germany). A third sequential imaging system also available consists of two scanners located in two separate rooms where the patient is transferred from the examination bed of one scanner to the other through a "shuttle" system. In our hospital we implemented a sequential hybrid PET/MRI that combines a 3T MRI and a time-of-flight PET scanner (Philips Ingenuity TF PET/MRI), separated by approximately 3 meters and located on each side of the

M.-I. Vargas (✉) · K. Lovblad
Neuroradiology, Geneva University Hospitals,
4 Gabrielle-Perret-Gentil, 1211 Genève, Switzerland
e-mail: maria.i.vargas@hcuge.ch

M. Becker · P. Loubeyre · J. Gariani · J.-P. Vallée
Radiology, Geneva University Hospitals,
4 Gabrielle-Perret-Gentil, 1211 Genève, Switzerland

V. Gariboto · O. Ratib
Nuclear Medicine, Geneva University Hospitals,
4 Gabrielle-Perret-Gentil, 1211 Genève, Switzerland

S. Heinzer
Philips AG Healthcare, Allmendstrasse 140,
8027 Zurich, Switzerland

examination table. The design and the performance of this device are described in detail in a recent publication [6]. In a clinical environment, a diagnostic MRI is first acquired, followed by MRI images for PET attenuation correction after which the patient is moved into the PET scanner for scanning. While this design does not allow simultaneous acquisition of the two modalities, it resembles current PET/CT scanners in its design. Provided that the patient does not move between imaging studies, it allows accurate fusion of coregistered PET and MRI sequences acquired sequentially.

The current paper comprises an overview of optimized clinical protocols for different organs using our sequential hybrid PET/MRI system. Particular attention is given to problems encountered in a clinical setting and their solutions, as used by specialists in neuroradiology, head and neck and breast oncology, and prostate imaging.

The major advantage in using these two techniques together consists in effectively combining the complex information from the two modalities, therefore potentially allowing a more accurate diagnosis. On one hand, MRI allows us not only to obtain anatomical information but currently enables identification of networks in the brain and functional imaging. The study of metabolism in tumors and epilepsy is possible with the utilization of sequences such as perfusion without contrast media using arterial spin labeling [7], with classic susceptibility perfusion and with diffusion-weighted imaging (DWI). However, in many cases such as in epilepsy, neurodegenerative diseases and oncological processes [8], PET imaging can provide additional metabolic and molecular information that can be valuable for a more accurate diagnosis [9, 10].

A variety of problems and technical challenges were encountered during the optimization of clinical protocols: first, those inherent to the scanner hardware itself, second, those caused by the long duration of studies, and third, related to the required training of medical and technical staff from the radiology and nuclear medicine departments. The duration of the study has an important impact on patient comfort and thereby on potential motion artifacts and is also associated with changes in the biodistribution of radiotracers, such as their accumulation in the bladder, which affects correct interpretation of image fusion in the pelvic area.

The first part of this review article describes general practical problems and technical challenges that can be encountered in clinical application of this new hybrid technique, and the second part focuses on issues that are specific to each organ system or clinical specialty.

Patient population

Two hundred and twenty-one patients (133 males; 88 females, mean age 59.7 years, range 7–90 years) were

scanned from April 2011 to January 2012. The anatomical regions evaluated were as follows: abdominal = 7, heart = 11, brain = 29, whole body = 31, head and neck = 27, breast and female pelvis = 46 and prostate = 70.

Scanning time and sequential PET/MRI protocols

The imaging protocols for the current PET/MRI system were developed in analogy to clinical MRI protocols used to assess diseases in various anatomical regions. As in clinical routine, an MRI examination may last between 30 and 70 min depending on the indication and the additional use of functional sequences. Simply adding an additional total body MRI for attenuation correction, total body diagnostic MRI sequences, and a total body PET acquisition would result in an unacceptably long examination time in clinical practice. Consequently, all protocols had to be shortened while maintaining diagnostic quality. In our institution, imaging protocols and quality control of PET/MRI exams are managed jointly by the senior radiologist and the senior nuclear medicine specialist, who also supervise senior residents in training who are present at the scanner console during the examination. Due to the importance of quality control and complexity of imaging protocols, technicians are instructed to check with attending physicians for the diagnostic adequacy of the study before discharging the patient. The attending staff then checks image quality and decide whether additional sequences may be required or if additional optional sequences available for a given protocol may be unnecessary. Despite this continuous monitoring of the examination by the attending staff, the total examination time including patient positioning, injection of radiotracer, MRI acquisition, table rotation, and PET scanning was on average 2.33 h (range: 1.52–3.08 h). In our series, the total examination time varied depending on the anatomical region being examined as follows: abdomen = 2.07, heart = 2.27, brain = 2.46, whole body = 2.07, head and neck = 3.08, prostate = 2.53, breast = 1.52, uterus and ovaries = 2.09.

PET imaging

The administered radiotracer activities have been established for the different indications following international guidelines and previous publications [11–14] and are in agreement with the national Swiss diagnostic reference levels.

The acquisition time was adapted to the different protocols: longer acquisition time was used on specific organs, depending on the clinical indication, while the shortest acquisition time recommended by the vendor (1 min 20 s)
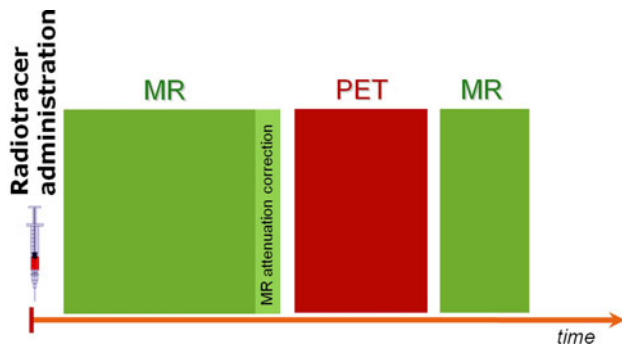
Fig. 1 PET/MRI workflow. The study typically begins with the acquisition of MRI sequences during the PET uptake time in order to reduce the overall duration of the exam (for details see text). After the diagnostic MRI, an MRI attenuation correction sequence is performed. Subsequently the table is rotated in order to acquire the PET images. If additional MRI sequences are necessary, a second table rotation to the MR position is realized followed by a second set of MRI acquisitions. Depending on the clinical indication, dedicated MRI coils are used

was used for whole body imaging. The datasets were reconstructed using a 3D listmode-based TOF ordered subset expectation maximization (OSEM) algorithm with 33 subsets and 3 iterations and a reconstruction resolution of 4 mm.

It should be noted that for the Gemini PET system, the time-of-flight technology and the use of an overlap of 50 % of bed positions allow shorter acquisition times as recommended [14].

The attenuation correction procedure, which is MR-based, is described in detail in a recent publication [6]. The attenuation map is obtained by automatic anatomical segmentation obtained from a specific whole-body MR sequence, consisting of a fast multi-stack spoiled T1-weighted gradient echo whole-body protocol that takes about 3 min for a 100 cm axial coverage. According to our standard protocol, this sequence is performed systematically just before table rotation and PET acquisition, in order to minimize artifacts due to motion and possible misregistration. A schematic representation of a PET/MRI acquisition is provided in Fig. 1.

Specific imaging protocols:

An overview of the specific protocols used for the PET/MRI acquisitions in different anatomic areas is given in Table 1.

Neuroradiology

Indications for hybrid imaging were: tumors (Fig. 2) ($n =$ 11), epilepsy (Fig. 3) ($n = 10$), and neurodegenerative diseases ($n = 8$). Depending on the clinical indication as

mentioned above, the protocols (Table 1) included: spin echo T1-weighted images (SET1, TE 10 ms, TR 520 ms, slice thickness 4 mm), Turbo spin echo T2-weighted images (FSET2 TE 100 ms, TR 4,000 ms, slice thickness 4 mm), 3D Fluid attenuated inversion recovery (3D FLAIR, TE 300 ms, TR 4,800 ms, slice thickness 1 mm), arterial spin labeling (ASL, TE 14 ms, TR 300 ms), classic susceptibility perfusion and diffusion tensor imaging (DTI, TE 72 ms, TR 7,800 ms, 30 directions) using an 8-channel brain coil.

For the evaluation of the resting glucose metabolism in the brain we administered 250 MBq of FDG in a dimly lit room with the patient in a supine position and 30 min later, we acquired a static brain PET acquisition lasting 10–15 min [12].

For brain tumor staging, we acquired a 10 min static brain PET acquisition 30 min after injection of 200 MBq of 18F-Fluoro Ethyl Tyrosine (FET) [11]: the uptake phase was performed while the patient was in the PET/MRI tomograph and was used for acquiring MRI sequences in order to shorten total scanning duration. The datasets were reconstructed using a 3D RAMLA [15] algorithm and a reconstruction resolution of 2 mm. Fusion of the MRI sequence and PET data was done routinely using the dedicated PET/MRI software (Philips Fusion Viewer on Extended Brilliance™ Workspace), as well as OsiriX medical imaging software (OsiriX v4.0 64bits; Geneva, Switzerland).

Head and neck

The indications in head and neck imaging included staging of primary and recurrent tumors (Figs. 4, 5) ($n = 20$) and follow-up of patients with high risk of recurrence after combined chemoradiotherapy with or without surgery ($n = 7$). The MRI examination of the head and neck area was done prior to the PET acquisition, starting immediately after the administration of the radiotracer. The duration of all head and neck MR sequences was 40–45 min. The protocol concept was similar to the one validated on other MR machines used clinically for head and neck oncology in our department. The coil used was the standard 16-channel head and neck phased array coil. The sequences performed routinely included: axial T1- (TE 16 ms, TR 683 ms) and T2 (TE 90 ms, TR 3528 ms)-weighted high resolution turbo spin echo sequences, a coronal STIR sequence (TE 80 ms, TR 5040 ms) an axial echo planar diffusion-weighted sequence (TE 260 ms, TR 3876 ms), and post-injection of Gadolinium chelates, axial and coronal T1-weighted turbo spin echo sequences, a 3D THRIVE (TE 6.9 ms and TR 3,4 ms) and a 3D T1 Dixon sequence (TE[1] 1,11 ms; TE[2] 2,0 ms, TR 3,3 ms). The slice thickness for the turbo spin echo sequences was 3–4 mm, for the 3D Thrive sequence 0.6 and

Table 1 Principal parameters in the optimization of workflow for a sequential MR-PET scanner

Organs	Clinical indications	Sequences	Plane	TR/TE (ms) Res (mm)	Routine sequences fusion	Total scanning time (hours)[b]	Total examination time (hours)
Brain	Tumor, epilepsy, and neurodegenerative diseases	FSE T2	Axial	4000/100 0.34/0.34/4.00	3DT1 + C, 3DFLAIR	1h00	2.46
		SET1 −/+ C	Axial	520/10 0.3/03/4.00			
		DTI	Axial	7800/72 1.88/1.88/2.00			
		3D FLAIR	3D	4800/300 1.1./1.10			
		ASL	Axial	300/14 3.75/3.75/7.00			
		3DT1FFE + C	3D	7.5/3.5 1.10./1.10/ 1.20			
Head and neck[a]	Staging of primary and recurrent tumors and follow-up of patients with high risk of recurrence after combined chemoradiotherapy	T2 FSE	Axial	3528/90 050/071/3.00	T2, 3 DT1FFE Dixon	1.11 + 0.36	3.08
		T1 FSE −/+ C	Axial	683/16 0.65/0.78/3.00			
		DWI (STIR, EPI)	Axial	3876/260 1.98/2.02/3.00			
		STIR TSE	Coronal	5040/80 (TI = 200) 0.60/0.80/4.00			
		3D T1 FFE DixonWB + C	3D	3.3/1.11/2.00 1.61/1.66/6.00			
Prostate[a]	Cancer staging in patients with a positive biopsy	T2 FSE	Axial, sagittal	4400/120 0.50/0.56/3.00 4000/120 060/0.68/3.00	3D T2FSE WB	1.17 + 0.36	2.53
		3DT2 FSE	3D	2000/181 0.51/0.51/3.00			
		DWI 0,500,1000,1500 b	Axial	3082/66 1.39/1.39/ 3000			
		3DT1 FFE Dixon + C	3D	3.2/1.11/2.0 1.61/1.66/6.00			
		Dynamic thrive (T1FFE) + C	3D	6.9/3.4 073/0.73/1.50			
Breast[a]	Locoregional staging of primary and recurrent breast tumors as well as the detection of distant metastases	3DT1 FFE (Dixon) −/+ C	3D	5.9/1.42/2.6 0.67/0.67/1.00	3 DT1 FFE Dixon WB	0.36 + 0.36	1.52
		T2 FSE	Axial	5000/120 059/059/3.00			
Whole body (WB)	Detection of distant metastases	T2 FSE (5 times to cover WB	Axial	3280/76 1.47/1.46/8.00	T2 FSE, Dixon WB	0.36	
		DWI	Axial	3949/29 1.46/1.45/7.00			
		Dixon WB	Axial	3.2/1.11/2.00 0.85/0.85/3.00			

TSE turbo spin echo, *SE*: spin echo, *DTI* diffusion tensor imaging, *DWI* diffusion-weighted imaging, *GE* gradient echo, *FLAIR* Fluid Attenuated Inversion Recovery, *DCS* dynamic susceptibility contrast, *FFE* fast field echo, *STIR* short TI inversion recovery, *C* contrast; *TR* repetition time, *TE* echo time, *Res* resolution

[a] Head and neck, prostate and breast are realized together with whole body PET-MR

[b] The total scanning time is the sum of the acquisition time of all sequences, whereas the total examination time includes—in addition to the scanning time—patient positioning, injection of gadolinium, injection of radiotracer, table rotation and breaks between sequences

2 mm for the Dixon sequence which enabled robust fat suppression. The area covered was from the skull base to the upper mediastinum (aortic arch) and the field of view was 24 cm. For all indications, the turbo spin echo sequences and the Dixon sequence were obtained routinely whereas the 3D Thrive sequence was performed only in oral cavity and oropharyngeal tumors and if the tumor extended to the skull base. Particular attention was paid to the phase encoding gradient which was oriented in the anteroposterior direction to avoid flow artifacts projecting to the pharynx and larynx. Although placing the phase encoding gradient in the anteroposterior direction lengthens the duration of the sequence, flow artifacts do not project to the areas of interest (typically the larynx and pharynx), thus improving image quality especially in the infrahyoid neck. The exam was monitored by the attending radiologist who checked the correct placement of all sequences as well as image quality. In the presence of major dyspnea and mucous secretions, patients were asked to clear the throat and cough in between the sequences and to refrain from coughing and swallowing vigorously during sequence acquisition. In cases with severely degraded image quality (5 out of 27 head and neck patients, 19 %), the sequence was repeated after a short break and repeat instructions to the patient. This led to improved image quality in 4 of the 5 cases (80 %), reducing the percentage of degraded image quality to below 4 %. After the dedicated MRI examination of the head and neck, the fat suppressed gadolinium-enhanced Dixon sequence, as well as axial STIR images were acquired on the chest and abdomen to search for distant metastases. This was done using the integrated MR body coil.

For PET head and neck imaging, we administered 370 MBq of FDG for adult patients over 50 kg of weight, and we used adapted doses for inferior weights (EANM guidelines) [14]. The PET images were systematically started 1 h after intravenous administration. PET acquisition spanning from the mid-thigh to the thorax was done in 1 min and 20 s per bed position, while the head and neck region was explored with 2–3 bed positions lasting 6 min each, in order to increase sensitivity and signal-to-noise ratio. The datasets were reconstructed using a 3D listmode-based TOF OSEM algorithm [16] with 3 subsets, 3 iterations and a reconstruction resolution of 2 mm. MR images obtained with the 3D THRIVE and the Dixon sequence were fused with the images obtained from the PET acquisition using the proprietary software (Philips Fusion Viewer on Extended Brilliance^{TM} Workspace) and Osirix Medical software after which they were archived on the PACS system (see Table 1).

Breast and female pelvis imaging

The indication for the realization of a PET/MRI in breast ($n = 36$) was locoregional staging (Figs. 6, 7) of primary and recurrent breast tumors, as well as the detection of distant metastases. The MRI protocol included an axial T2 FSE(TE: 120 ms, TR 5000 ms) and a 3D T1 Dixon (TE1, 1.42 ms, TE2 2.6 ms, TR 5.9 ms) sequence acquired immediately, 1 and 6 min after intravenous administration of 0.2 ml/kg of a gadolinium chelate. Digital subtraction of the water-only Dixon images was performed using the dedicated MRI software and it is this sequence that was interpreted together with the PET images.

Indications for PET/MRI in the female pelvis ($n = 10$) were endometrial carcinoma and cervical cancer, mainly for the delineation of uterine extension and lymph node staging.

For PET-breast imaging, we administered 370 MBq of FDG for adult patients over 50 kg of body weight; doses were adapted for inferior weights (EANM guidelines) [14]. Approximately 20–30 min later, we started the dedicated breast MR sequences in prone position, using a 7-channel breast coil with a built-in template for PET attenuation correction, followed by a prone PET acquisition of 2 min 15 s per bed position (usually 2). The PET acquisition started systematically 1 h after FDG administration. Reconstruction was performed using a 3D listmode-based TOF OSEM algorithm with 33 subsets and 3 iterations and a reconstruction resolution of 4 mm. Subsequently, a supine whole-body MR and PET (1 min 20 s per bed, from the feet towards head) were acquired. Fusion of the subtraction MR sequence and PET data was done routinely using the dedicated PET/MRI software (Philips Fusion Viewer on Extended Brilliance^{TM} Workspace) as well as Osirix Medical fusion software (see Table 1).

Prostate imaging

The main indication for PET/MRI was prostate cancer staging in patients with a positive biopsy (75 %) (Figs. 8, 9). Other indications included the assessment of tumor recurrence after treatment in patients with increasing serum prostate specific antigen (PSA) (15 %), and tumor detection in patients with increased PSA but negative biopsies (10 %). The following protocol was used: axial and sagittal T2-weighted fast spin echo (FSE, TE 120 ms, TR 4400 ms) sequence with a resolution of $0.3 \times 0.3 \times 3$ mm using both an endorectal and the 6-channel SENSE cardiac coil. After removal of the endorectal coil, the following MR acquisitions were performed using a phased array coil only: a 1 mm isotropic T2 3D fast spin echo (TE 181 ms, TR 2000 ms), an axial diffusion-weighted sequence with b values 0, 500, 1000 and 1500, as well as a dynamic 3D T1 fat saturated field echo sequence (TE 3,4 ms, TR 6,9 ms) during the injection of Gd contrast agent (Dotarem 0.1 mmol/kg). Finally, using the integrated body coil, 5
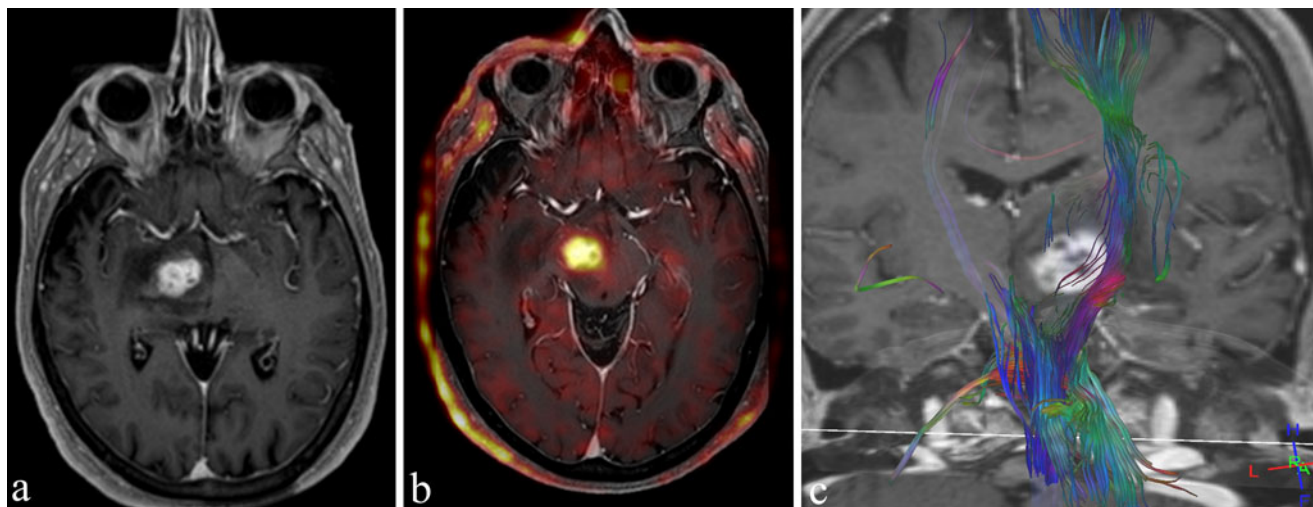
Fig. 2 Patient with glioblastoma at the mesencephalon level; note the enhancement (**a**), the increase of metabolism of the18F fluoroethyl-L-tyrosine on fused PET/MRI-images (**b**) and the cortico-spinal tract fibers displaced by the tumor on the tractography sequence (**c**)

Fig. 3 Artifacts of inhomogeneity and movement, in a patient wearing an MR-compatible EEG recording system. The PET/MRI examination was performed for presurgical evaluation of epilepsy and for this reason associated with EEG monitoring. Artifacts of inhomogeneity of signal are illustrated on an axial FLAIR image (**a**) with associated motion artifacts. Axial FLAIR sequence of the same patient obtained 15 days earlier on other scanner (**b**)
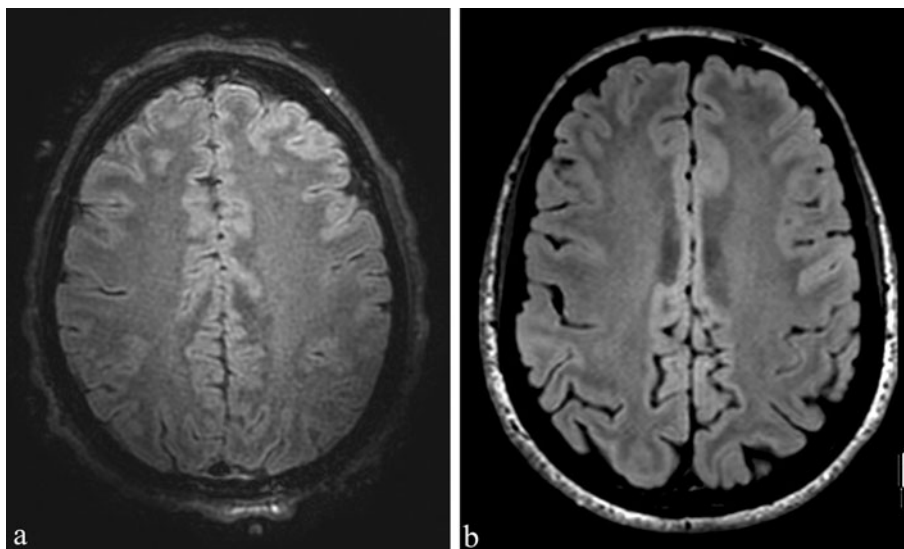
batches of 3D T1 fat saturated field echo sequence were acquired on the upper abdomen to search for lymph nodes.

For PET-imaging of the prostate we adapted the protocol previously validated for PET/CT investigations [14]. Scanning started with a dynamic acquisition of 10 min centered on the prostate with the injection of 300 MBq of 18F-Fluorocholine, followed by a whole-body acquisition (1 min 20 s per bed, from feet toward head), and subsequently by a dedicated 2 bed acquisition on the pelvis, lasting 5 min per bed. These images were reconstructed using a 3D listmode-based TOF OSEM algorithm with 33 subsets, 3 iterations and a reconstruction resolution of 4 mm.

Problems and limitations common to all examinations

The following problems were encountered:

Scanning time

In order to decrease scanning time, each protocol was adapted to decrease the number of sequences to the minimum necessary for diagnosis. This was done after retrospective analysis of the available cases. For example, in the head and neck, the total body MRI protocol for the detection of distant metastases included a STIR sequence and a Dixon sequence after the intravenous administration of Gadolinium. After retrospective analysis of all
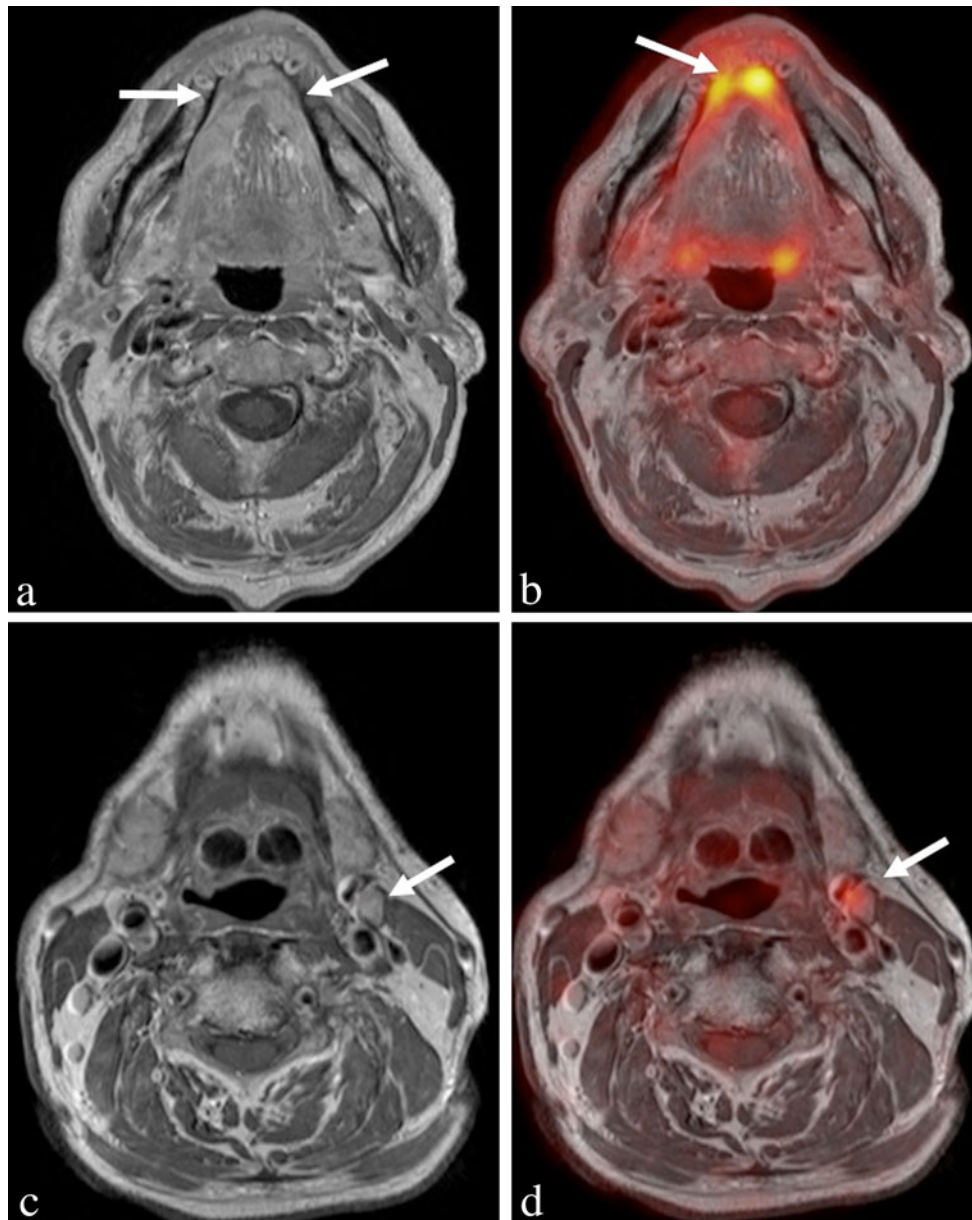
Fig. 4 PET/MRI with FDG obtained in a patient with a tumor of the mouth floor. The contrast enhanced T1-weighted MR images are shown in **a**, whereas the image fusion between the T1-weighted images and the PET acquisition is shown in **b**. The tumor invades the anterior floor of the mouth bilaterally (*arrows*) extending into the sublingual spaces and the geniohyoid muscles. There is an abnormal level 2 lymph node on the left, as seen on the MR image (**c**, *arrow*). Note the perfect match between the PET and the MRI images both for the tumor and for the lymph node, which show an increased metabolism (*arrows* on **d**). Histology revealed squamous cell carcinoma

available head and neck cases, we found that the STIR sequence for the chest and abdomen did not yield additional information, as compared to the Dixon sequence and the PET acquisition. Consequently, we do not perform the STIR sequence anymore to look for distant metastases but instead rely on the Dixon and fused PET-Dixon sequence. Further analysis of cases will also help to identify other MRI sequences that might be redundant when the metabolic-molecular information of PET is available, obtaining additional reduction in the duration of the entire exam. Nevertheless, the long scanning time remains a serious problem in clinical practice, particularly in patients with pain, dyspnea, dysphagia and cognitive problems. In cases where full patient cooperation is possible, such as in the head and neck, short pauses between the sequences, where patients can cough and
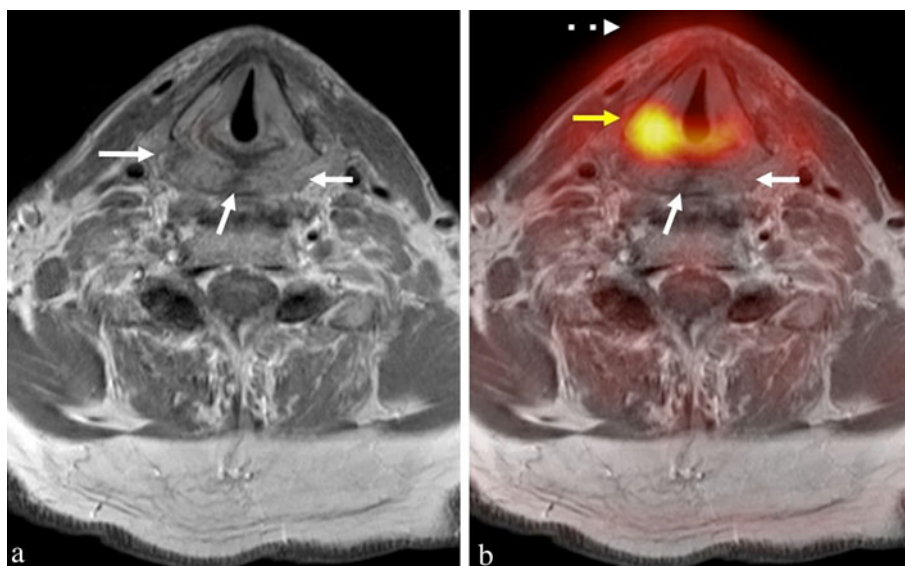
Fig. 5 PET/MRI with FDG obtained in a patient with suspected recurrence after chemoradiotherapy. T1-weighted contrast-enhanced axial MR image (**a**) and corresponding fused PET MRI image (**b**). The MR image shows a recurrent tumor arising from the hypopharynx (*white arrows*). Due to patient movement, the PET image is displaced anteriorly (*dashed arrow*) resulting in poor PET MR fusion. Based on the fused image, one would interpret the hypermetabolic area in the larynx at the level of the right vocal cord and at the level of the posterior commissure (*yellow arrow*) as a recurrent tumor, whereas the MR image clearly indicates that the recurrent tumor is not in the larynx but in the hypopharynx, therefore having a major impact on the surgical resection. Surgical biopsy confirmed tumor recurrence within the hypopharynx

Fig. 6 Invasive ductal carcinoma of 12 mm of size with perfect fusion between MRI and PET-FDG and very good correlation with pathology
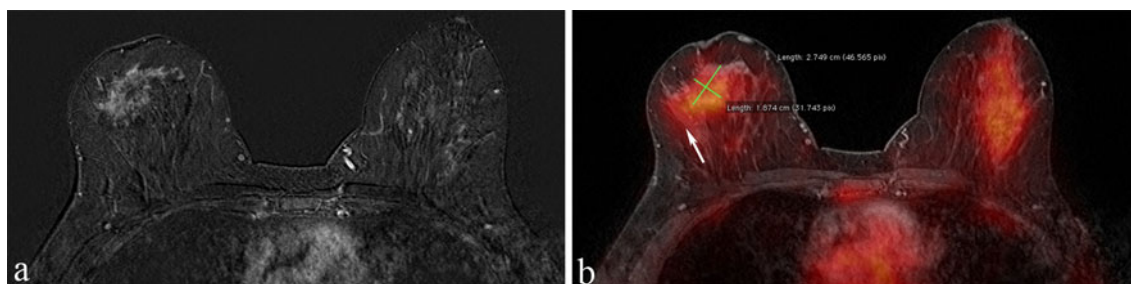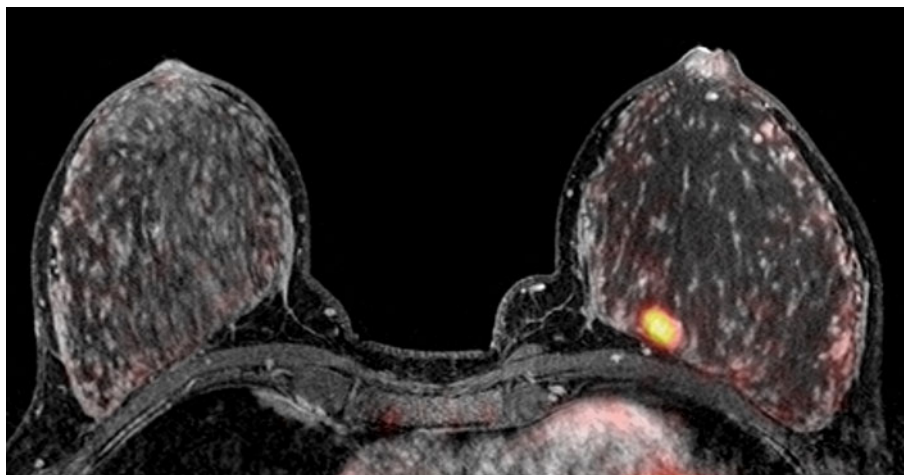

Fig. 7 Invasive lobular carcinoma of 50 mm of size (**a**); note slight defect of fusion between MRI and PET-FDG images (*arrow*, **b**)
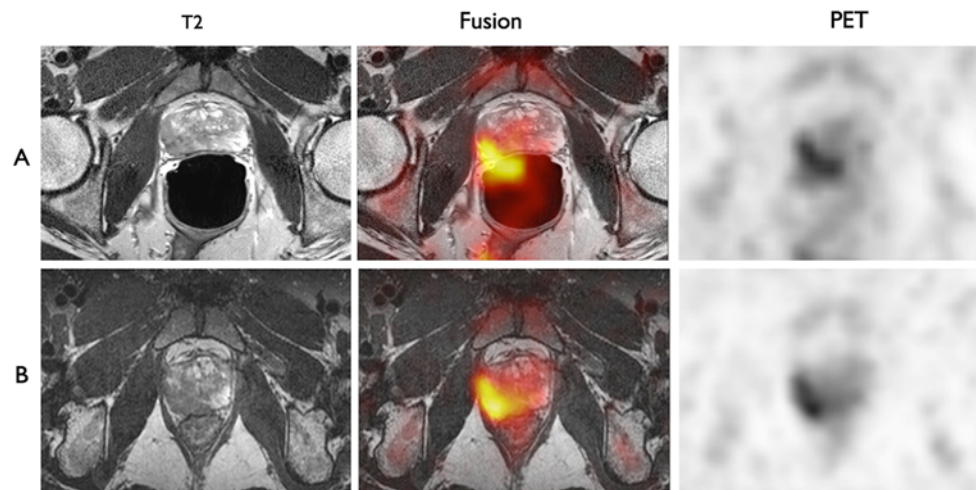
Fig. 8 Effect of the endorectal coil on the PET/MRI registration. On the left, axial T2 images of a prostate with a large right peripheral zone cancer, as demonstrated by a hypointense area. The tumor is visible on both the T2-weighted images acquired with an endorectal coil (row **a** *left*) and on the images obtained with an external phased-array coil (row **b** *left*). On the PET images, the tumor is characterized by an increased 18F-Fluorocholine metabolism. The fusion between the T2-weighted images and the PET images is not accurate when the T2-weighted images are acquired with an endorectal coil. Using an external phased array coil results in an almost perfect matching between the PET and T2 images
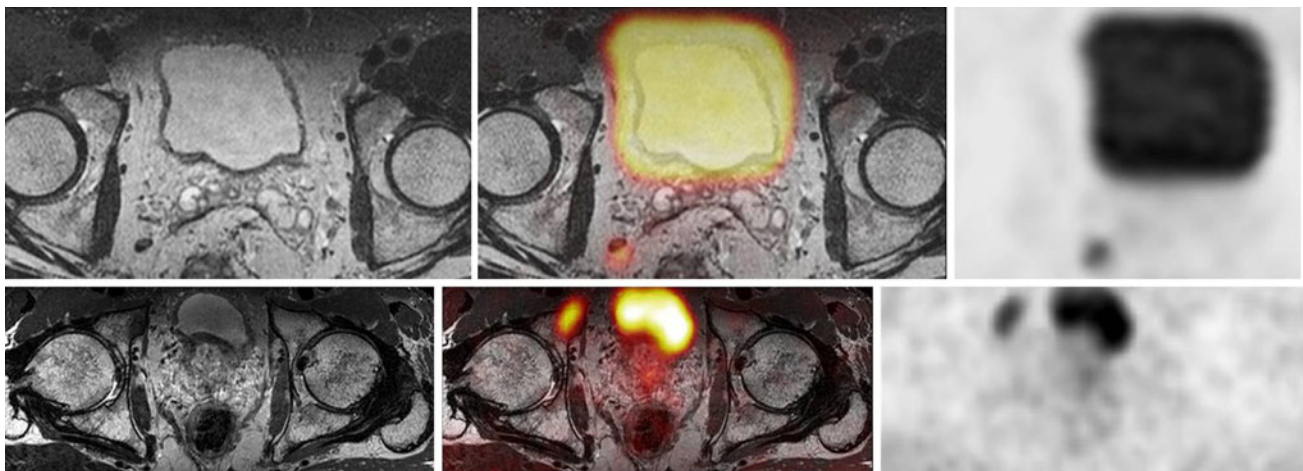

Fig. 9 Example of correct and low quality fusion of PET and MRI images due to different bladder filling. In the upper row, PET data were acquired after the MRI data and bladder distension was more important on the PET images, resulting in an inaccurate fusion of both imaging modalities. As a result, the PET with 18F-Fluorocholine signal uptake of the abnormal lymph node just behind the right seminal gland is shifted posteriorly. This misregistration related to bladder filling was solved by restricting water intake 4 h before the PET/MRI exam and by asking the patient to void just before beginning the image acquisition. This simple measure ensures a correct fusion in most cases as demonstrated in the lower row. Please note the perfect matched MRI and PET signal from the bladder as well as from the bone metastasis in the right pubic ramus

clear the throat are a potential solution to avoid subsequent motion artifacts and poor image quality. These short breaks enable patients to refrain from vigorous coughing during scanning but increase the overall duration of the exam. While it is true that these short breaks might potentially increase misalignment, they are absolutely necessary in order to achieve good quality MR images.

Motion artifacts

This type of artifact was mainly observed in long studies (Fig. 3). It was partially solved by decreasing the total number of sequences and by using motion correction algorithms [17, 18]. We also used contention devices and tried to use body positions in which the patient was the most comfortable (i.e. arms down instead of the arms up

position that is used for PET/CT). We also routinely explain to the patients the importance of the absence of movement in order to increase their awareness and obtain the best possible collaboration.

Quality control

The PET scanner detector pairs are inherently not uniform in PET systems due to a systematic variation of detector pair geometry from the center to the periphery of the FOV, a drift in photomultiplier gains and nonuniform sampling across the FOV [19].

Therefore, daily automated calibrations of the PET electronics have to be performed, which include the following: (1) voltage and current tests for the PET gantry electronics to ensure accurate digitization of the signal; (2) baseline correction for the analog offsets of the photomultiplier channels and gain calibration to ensure that all photomultipliers amplify equally; (3) a timing test for the time-of-flight circuitry. After these hardware calibrations, emission sinograms are collected in order to identify system drifts affecting image quality and/or defective hardware.

Monthly quality controls are performed by physicists for PET and MRI to ensure uniformity of the system over the entire FOV and to calibrate and validate standardized uptake values (SUVs) so that subsequent patient scans can be quantified properly.

Accurate image fusion in PET/MRI

Initial system calibration

For the successful fusion of PET and MRI images, the physics of the MR device needs to be taken into account. Unlike in CT and PET, where the absolute image position is largely determined by the hardware, the center of an MR image depends on accurate determination of the Larmor frequency of the spins, f0. This calibration is automatically performed at the beginning of each MR acquisition but may be less reliable in the presence of heavy frequency differences across the FOV (i.e. broad frequency peak if materials containing metal are used). Therefore, in order to perform initial image alignment calibrations, probes that are visible on MR and PET [20] consisting of MR compatible materials were chosen by the vendor. This allows accurate frequency determination and avoids image distortions of the MR image, which can occur in addition to positioning offsets.

Patient scans

MR images are prone to suffer from distortions which occur both from machine-dependent and patient-dependent

effects, such as magnetic field inhomogeneities, chemical shift and eddy currents [21]. Applications of paired positive and negative (bipolar) gradients, as well as twice refocused spin-echo sequences can be used to minimize eddy current effects, for example in diffusion-weighted sequences, whereas when using spin-echo sequences instead of gradient echo sequences, one can minimize distortions that are induced by differences in susceptibility (i.e. at the air/tissue interfaces, metal implants). Setting a large receiver bandwidth helps to reduce chemical shift artifacts that may occur when different resonant frequencies are present in the FOV (i.e. water and fat), albeit at the expense of a reduced SNR and longer scan times.

These sequence-, hardware- and patient-related effects need to be taken into account when acquiring MR images that will be fused with PET. Whereas machine-related effects are corrected for using a phantom of known geometry during system calibration, patient-related effects have to be taken care of by using dedicated correction algorithms in the fusion software and adapted MR sequence parameters. To reduce patient-related effects and to minimize fusion artifacts on our system, we used Dixon sequences for whole-body and H/N PET/MRI scans [22]. Using this sequence, the chemical shift offsets between water and fat are corrected for during the reconstruction process so that the absolute image position of both the water and fat images are correct. This then leads to an improved image overlay between all types of Dixon MRI images (water, fat, in-phase and out-of-phase) and PET images. In addition to the Dixon sequence, spin-echo sequences proved to be particularly robust for imaging the H/N area.

General MR artifacts

MRI artifacts observed in our hybrid PET/MRI system were similar to MRI artifacts reported in dedicated non-hybrid MRI units [22] and included magnetic susceptibility artifacts, blood-flow artifacts, and homogeneity artifacts. We did not observe any truncation or Gibbs artifacts in the current series. In a recent study evaluating 2,705 brain MRI studies performed on a 3T machine from a different vendor [23], the authors found that among all artifacts identified, 29 % were magnetic susceptibility artifacts, 57 % were pulsation artifacts, 3 % were homogeneity artifacts, and 6 % motion artifacts [22]. In the current series of 29 brain studies, we have observed these artifacts in four patients (14 %). They typically occurred on the 3DT1, 3DFLAIR and ASL sequences.

Data regarding the prevalence of artifacts in hybrid PET/MRI systems in larger clinical series are currently lacking. Delso et al. [24] reported a good overall performance of a simultaneous integrated PET/MRI system (Biograph mMR, Siemens) during independent and simultaneous acquisition of MRI and PET data on a phantom. In particular, spatial resolution, scatter fraction, count losses, image quality,

geometric accuracy, signal to noise ratio, field homogeneity and radiofrequency noise were within the tolerances defined by the American College of Radiology; the results were also similar to data of state-of-the-art PET/CT scanners with regard to the PET acquisition. However, in vivo measurements were performed only in one patient and in a single healthy volunteer [24].

Technical staff

In our setting, the hybrid PET/MRI is operated by two technicians in the routine clinical setting while physicists assist with the development and implementation of new sequences before these are used in clinical routine. While in Switzerland technicians are trained and certified to operate both nuclear medicine and radiological devices, we elected to match two teams of experienced technologists with different backgrounds: one group of technologists with at least two years of clinical experience in MRI imaging and one with a similar specific experience in PET imaging. On site technician training can be lengthy, as each technician had to learn the basic principles of the technique that he did not routinely perform prior to the introduction of the PET/MRI machine in our department. This required instruction by specialized personnel in order to provide the needed special training of theoretical and practical aspects of MRI physics, nuclear medicine principles and applications, as well as radioprotection issues. In addition, the supervision of the exam required a complex organization structure because both modalities had to be checked and supervised by different individuals of the multidisciplinary team for accurate positioning of MRI sequences in view of optimized protocols. Although it is very difficult to estimate the added burden of such organization, it is clear that at the current stage of development of this new technique, each PET/MRI exam needs to be tailored and monitored to ensure adequate diagnostic quality and therefore requires supervision by the medical staff, in particular for adapting the protocol depending on radiologic findings and patient cooperation. Close collaboration between the medical and technical teams as well as physics staff of both departments of Nuclear Medicine and Radiology is essential to assure the shortest possible examination time, while providing the best quality of each modality to insure adequate quality for joint image interpretation.

Specific problems inherent to each organ system

Nervous system

For nervous system examinations, the most relevant specific problems that were encountered included the long scanning time, susceptibility artifacts (two cases due to an implant (ventriculo-peritoneal drain) and motion artifacts (two cases) (Fig. 3). They typically occurred in the 3DT1, 3DFLAIR and ASL sequences.

Gynecological imaging

For gynecological imaging, the most relevant problems encountered were due to occasional misalignment fusion artifacts (Fig. 7). In the lower abdominal region, motion and organ shift would result in misalignment of PET and MR images.

Head and neck imaging

Due to the choice of the phase encoding gradient in the anteroposterior direction, flow related artifacts over the relevant areas to be assessed (pharynx and larynx) were practically nonexistent and yielded images of good and reproducible image quality. This was of particular importance for the interpretation of MR studies involving tumors of the larynx, hypopharynx or oropharynx [25]. Similar to data published in the literature [25], we found that spin echo sequences were particularly robust to motion caused by swallowing and breathing and to field inhomogeneity caused by air–soft tissue interfaces. Unlike spin echo sequences, gradient echo sequences require gradients to dephase and rephase the spins to create the signal echo. They are therefore more sensitive to inhomogeneities since spin dephasing is then not compensated with the refocusing gradients. This leads to a lower SNR than in spin echo sequences. Of the 27 patients who underwent a PET/MRI examination, images were considered to be of poor quality only in three cases (11 %) due to major patient movement and subsequently poor fusion, making interpretation of images nearly impossible. In addition, slight motion or changes in the head and neck position between the MR and the PET acquisition resulted in suboptimal fusion (Fig. 5) in four cases (15 %), in particular when dealing with small structures such as lymph node metastases inferior to 1 cm or small sized head and neck tumors (maximum diameter less than 2 cm). One particular problem was that due to the impaired fusion quality, it became very difficult to estimate the size of the tumor (delineation with MRI alone or with fused PET MR was more precise) (Fig. 5). Susceptibility artifacts related to dental fillings and implants are a problem that may typically occur in the head and neck. They are seen not only on the diagnostic MRI images but also propagate on the atMRI. In our series, we observed severe artifacts related to dental implants in four head and neck cases (15 %). However, evaluation of tumor spread was not possible only in one case (3 %), in which a

previous CT and a 1.5 T MRI were also nondiagnostic with respect to precise presurgical evaluation of submucosal tumor extent.

Prostate imaging

Regarding prostate hybrid imaging, the most important artifacts were related to patient motion during the examination. Special instructions were given to patients to avoid voluntary movements during the acquisition. In clinical routine, the endorectal coil was removed after anatomical T2 acquisition to decrease motion related to the patient discomfort. In addition, removing the endorectal coil decreased susceptibility artifacts in the posterior zone of the prostate mainly on the diffusion-weighted MRI sequence, resulting in an improved image quality. Our tests showed that when T2 MRI images are acquired with the endorectal coil in place, the registration between PET and MR images is inaccurate (Fig. 8). Therefore, whole-body T2 images used for attenuation correction and for anatomical localization are acquired after endorectal coil removal while using an external phased array coil. In order to avoid blurred images due to bowel movement, anti-peristaltic drugs (Buscopan®) were routinely administered subcutaneously. During the first cases that we examined, we observed that filling of the bladder during the hybrid exam may result in poor alignment of MRI and PET images of the prostate region (Fig. 9). We are therefore now asking the patients to stop drinking 4 h before the exam and to void their bladder before starting the exam.

Conclusion

PET/MRI is a recent technique increasingly used in clinical practice with two main advantages: first, reduction of total radiation dose by avoiding the CT acquisition necessary in hybrid PET/CT machines, and second, combined metabolic and anatomical information in a single imaging session taking advantage of the superior soft tissue characterization of MRI over CT.

The results of our first clinical experience show that in order to achieve optimum impact and ensure clinical acceptance of this exciting new technology it is necessary to adapt and fine-tune existing imaging protocols to insure optimal diagnostic quality of both techniques during the acquisition of hybrid PET/MRI examination. In our institution, this was done by carefully monitoring the examinations while they were being performed: a joint effort of a multidisciplinary team consisting of technologists, radiologists, nuclear medicine specialists and application physicists was necessary to reach our goal.

For the MRI system, we mainly encountered artifacts related to metal implants and patient motion. The frequency of motion artifacts can be reduced by shortening the examination time, and optimizing imaging workflow and protocols. Simple tricks such as the use of robust sequences (spin echo and Dixon), breaks between the acquisition of sequences in dyspneic and coughing patients, anteroposterior phase encoding in the head and neck, administration of Buscopan, early removal of the endorectal coil and voiding the bladder before the exam in prostate cancer patients allow to obtain adequate results and good image quality in most patients. Furthermore, to obtain optimal image quality, it is important to apply meticulous daily quality control procedures of PET scanner calibration, as well as accurate MRI and PET alignment calibration.

We have reported herewith our first clinical experience with hybrid PET/MRI in a large series of patients referred for both diagnostic PET and MR procedures. The optimized protocols used to evaluate a variety of pathologies, and simple tricks and recommendations to improve image quality are presented and discussed. Further evaluation of clinical data and controlled studies evaluating the correlation with histology or patient outcome will show whether this new technology will have a significant impact on patient management compared to current state PET/CT, where these two types of imaging procedures are acquired separately on different devices at different points in time.

References

1. Shao Y, Cherry SR, Farahani K, Meadors K, Siegel S, Silverman RW, Marsden PK (1997) Simultaneous PET and MR imaging. Phys Med Biol 42(10):1965–1970
2. Woods RP, Mazziotta JC, Cherry SR (1993) MRI-PET registration with automated algorithm. J Comput Assist Tomogr 17(4):536–546
3. Ratib O, Beyer T (2011) Whole-body hybrid PET/MRI: ready for clinical use? Eur J Nucl Med Mol Imaging 38(6):992–995
4. Schlemmer HP, Pichler BJ, Schmand M, Burbar Z, Michel C, Ladebeck R, Jattke K, Townsend D, Nahmias C, Jacob PK, Heiss WD, Claussen CD (2008) Simultaneous MR/PET imaging of the human brain: feasibility study. Radiology 248(3):1028–1035
5. Catana C, Wu Y, Judenhofer MS, Qi J, Pichler BJ, Cherry SR (2006) Simultaneous acquisition of multislice PET and MR

images: initial results with a MR-compatible PET scanner. J Nucl Med 47(12):1968–1976

6. Zaidi H, Ojha N, Morich M, Griesmer J, Hu Z, Maniawski P, Ratib O, Izquierdo-Garcia D, Fayad ZA, Shao L (2011) Design and performance evaluation of a whole-body Ingenuity TF PET-MRI system. Phys Med Biol 56(10):3091–3106

7. Pendse N, Wissmeyer M, Altrichter S, Vargas M, Delavelle J, Viallon M, Federspiel A, Seeck M, Schaller K, Lövblad KO (2010) Interictal arterial spin-labeling MRI perfusion in intractable epilepsy. J Neuroradiol 37(1):60–63

8. Boss A, Stegger L, Bisdas S, Kolb A, Schwenzer N, Pfister M, Claussen CD, Pichler BJ, Pfannenberg C (2011) Feasibility of simultaneous PET/MR imaging in the head and upper neck area. Eur Radiol 21(7):1439–1446

9. Garibotto V, Vargas MI, Lovblad KO, Ratib O (2011) A PET-MRI case of corticocerebellar diaschisis after stroke. Clin Nucl Med 36(9):821–825

10. Garibotto V, Heinzer S, Vulliemoz S, Guignard R, Wissmeyer M, Seeck M, Lovblad KO, Zaidi H, Ratib O, Vargas MI (2012) Clinical applications of hybrid PET/MRI in neuroimaging. Clin Nucl Med. doi:10.1097/RLU.0b013e3182638ea6

11. Vander Borght T, Asenbaum S, Bartenstein P, Halldin C, Kapucu O, Van Laere K, Varrone A, Tatsch K (2006) EANM procedure guidelines for brain tumour imaging using labelled amino acid analogues. Eur J Nucl Med Mol Imaging 33(11):1374–1380

12. Varrone A, Asenbaum S, Vander Borght T, Booij J, Nobili F, Nagren K, Darcourt J, Kapucu OL, Tatsch K, Bartenstein P, Van Laere K (2009) EANM procedure guidelines for PET brain imaging using [18F] FDG, version 2. Eur J Nucl Med Mol Imaging 36(12):2103–2110

13. Steiner C, Vees H, Zaidi H, Wissmeyer M, Berrebi O, Kossovsky MP, Khan HG, Miralbell R, Ratib O, Buchegger F (2009) Three-phase 18F-fluorocholine PET/CT in the evaluation of prostate cancer recurrence. Nuklearmedizin 48(1):1–9

14. Boellaard R, O'Doherty MJ, Weber WA, Mottaghy FM, Lonsdale MN, Stroobants SG, Oyen WJ, Kotzerke J, Hoekstra OS, Pruim J, Marsden PK, Tatsch K, Hoekstra CJ, Visser EP, Arends B, Verzijlbergen FJ, Zijlstra JM, Comans EF, Lammertsma AA, Paans AM, Willemsen AT, Beyer T, Bockisch A, Schaefer-Prokop C, Delbeke D, Baum RP, Chiti A, Krause BJ (2010) FDG PET and PET/CT: EANM procedure guidelines for tumour PET imaging: version 1.0. Eur J Nucl Med Mol Imaging 37(1):181–200

15. Browne JA, De Pierro AR (1996) A row-action alternative to the EM algorithm for maximizing likelihoods in emission tomography. IEEE Trans Med Imaging 15(5):687–699

16. Hudson M, Larkin RS (1994) Accelerated image reconstruction using ordered subsets of projection data. IEEE Trans Med Imaging 13:601–609

17. Catana C, van der Kouwe A, Benner T, Michel CJ, Hamm M, Fenchel M, Fischl B, Rosen B, Schmand M, Sorensen AG (2010) Toward implementing an MRI-based PET attenuation-correction method for neurologic studies on the MR-PET brain prototype. J Nucl Med 51(9):1431–1438

18. Catana C, Benner T, van der Kouwe A, Byars L, Hamm M, Chonde DB, Michel CJ, El Fakhri G, Schmand M, Sorensen AG (2011) MRI-assisted PET motion correction for neurologic studies in an integrated MR-PET scanner. J Nucl Med 52(1):154–161

19. Hoffman EJ, Guerrero TM, Germano G, Digby WM, Dahlbom M (1989) PET system calibrations and corrections for quantitative and spatially accurate images. IEEE Trans Nucl Sci 36(1):1108–1112

20. Ng TS, Procissi D, Wu Y, Jacobs RE (2010) A robust coregistration method for in vivo studies using a first generation simultaneous PET/MR scanner. Med Phys 37(5):1995–2003

21. Langlois S, Desvignes M, Constans JM, Revenu M (1999) MRI geometric distortion: a simple approach to correcting the effects of non-linear gradient fields. J Magn Reson Imaging 9(6):821–831

22. Eggers H, Brendel B, Duijndam A, Herigault G (2001) Dual-echo Dixon imaging with flexible choice of echo times. Magn Reson Med 65(1):96–107

23. Vargas MI, Delavelle J, Kohler R, Becker CD, Lovblad K (2009) Brain and spine MRI artifacts at 3Tesla. J Neuroradiol 36(2):74–81

24. Delso G, Fürst S, Jakoby B, Ladebeck R, Ganter C, Nekolla SG, Schwaiger M, Ziegler SI (2001) Performance measurements of the Siemens mMR integrated whole-body PET/MR scanner. J Nucl Med 52(12):1914–1922

25. Becker M, Zbaren P, Casselman JW, Kohler R, Dulguerov P, Becker CD (2008) Neoplastic invasion of laryngeal cartilage: reassessment of criteria for diagnosis at MR imaging. Radiology 249(2):551–559